The effect of very high magnetic fields on the delayed fluorescence from oriented bacterial reaction centers

Richard A. Goldstein and Steven G. Boxer

Department of Chemistry, Stanford University, Stanford, CA (U.S.A.)

Delayed fluorescence is observed from quinone-depleted *Rhodobacter sphaeroides* reaction centers due to re-formation of the excited state of the special pair electron donor from the initially formed radical-pair state. Theoretical calculations based on the currently accepted scheme for the initial reaction dynamics predict quantum beats in the delayed fluorescence time evolution at very high magnetic field for oriented reaction centers. The delayed fluorescence was observed at magnetic fields from 1 kG to 150 kG using time-resolved single-photon counting. The reaction centers were oriented by insertion into phosphatidylcholine vesicles that were subsequently air-dried. Quantum beats were not observed, indicating that the reaction scheme may need revision. Saturation of the magnetic field effect on the delayed fluorescence lifetime was observed above 100 kG. The decay rate above saturation permits the first direct measurement of k_T, the rate of radical pair decay to the triplet state of the electron donor. We obtain a value for k_T of $(4.0 \pm 0.3) \cdot 10^8$ s^{-1}. The implications of this value of k_T and the absence of quantum beats at high field are discussed further in the accompanying manuscript (Biochim. Biophys. Acta 977 (1989) 78–86).

Theory

The initial charge separation in photosynthetic bacteria takes place in a membrane-bound chromophore-protein complex called the reaction center (RC). Charge separation is initiated by excitation of the primary electron donor (P) to its first excited singlet state (^{1}P). Within a few picoseconds an electron moves from P to I, the intermediate electron acceptor, to form the radical-pair state, P^+I^- [1,2]. When further electron transfer is blocked by prior reduction or removal of the quinone secondary acceptor, Q_A, the radical pair decays by charge recombination to re-form ^{1}P, decays to the ground state of P, or forms ^{3}P, the excited triplet state of the donor, depending upon the electronic spin state of the radical pair (see Fig. 1). An applied magnetic field can affect the evolution of this electronic spin state and thus affect the competition between spin-dependent decay pathways. In this way, it is possible to alter the

quantum yields and kinetics of any state whose formation or decay involves passage through the radical-pair state [3].

The radical-pair mechanism theory has been used successfully to analyze these magnetic field effects [4–6]. As shown in Fig. 1, the radical pair is initially formed
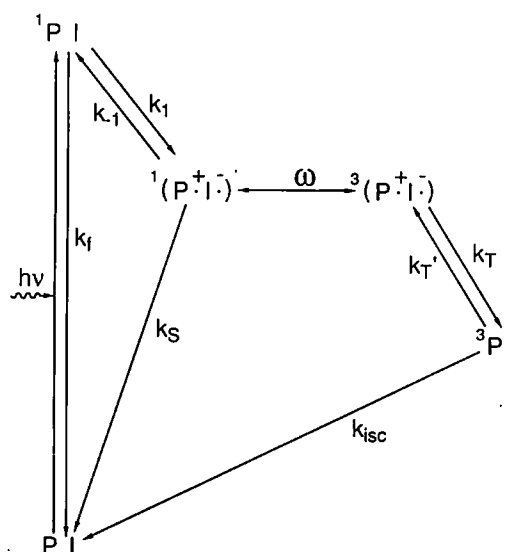

Fig. 1. Reaction scheme used to analyze reaction dynamics. k_f is the rate of fluorescence.

Abbreviations: RC, reaction center; P, primary electron donor; Q_A, quinone secondary acceptor.

Correspondence: S.G. Boxer, Department of Chemistry, Stanford University, Stanford, CA 94305, U.S.A.

from ^{1}P in a singlet spin configuration, denoted ^{1}(P$^+$I$^-$), with rate k_1. ^{1}(P$^+$I$^-$) can decay to P (rate k_S), reform ^{1}P (rate k_{-1}), or undergo coherent electron spin evolution at frequency ω to form the triplet spin configuration of the radical pair ^{3}(P$^+$I$^-$). ^{3}(P$^+$I$^-$) either decays by recombination to generate ^{3}P (rate k_T), or it evolves back to ^{1}(P$^+$I$^-$). At zero magnetic field, the nuclear hyperfine interaction causes interconversion of the singlet radical-pair state and all three triplet radical-pair states. When the magnetic field is increased from 0 to a few hundred gauss, the rate of interconversion decreases because of the loss of the near degeneracy of the singlet and two of the triplet radical-pair states. As the field is increased beyond 1 kG, the interconversion rate increases as singlet-triplet mixing due to the g-factor difference between P$^+$ and I$^-$, Δg, becomes important. The Δg effect becomes the dominant mechanism for interconversion at fields above 50 kG.

In addition to prompt fluorescence from ^{1}P, delayed fluorescence is observed due to repopulation of ^{1}P from ^{1}(P$^+$I$^-$) in RCs when subsequent electron transfer to Q$_A$ is blocked (k_f is the rate of fluorescence) [7–10]. The fluorescence wavelength maximum is approx. 910 nm at room temperature, shifting slightly to longer wavelength as the temperature is reduced [11]. In contrast to the time evolution of the absorbance changes due to the radical-pair state, which can be described by a single exponential [12–15], the time evolution of this delayed fluorescence has been described by sums of exponentials at zero and low fields [10,11,13,16,17]. This multi-exponential decay has been attributed to relaxation between distinct states, either different nuclear coordinate configurations of P$^+$I$^-$ [11] or different electronic states involving electron transfer to both the L and M branches of the RC [16]. Further implications of each of these additions to the reaction scheme of Fig. 1 are discussed in the accompanying paper [18].

An alternative hypothesis is that the complicated time evolution of the delayed fluorescence is due to the rather special combination of stochastic and coherent processes in the reaction scheme. As has not always been adequately considered, P$^+$I$^-$ can reform ^{1}P only while in the singlet electron spin configuration; consequently, the time evolution of the observed delayed fluorescence decay kinetics will not be the same as the time evolution of the radical-pair state as measured by absorption changes. The decay of the delayed fluorescence reflects the time evolution of the ^{1}(P$^+$I$^-$) state; in particular, assuming the scheme in Fig. 1 is correct and that $k_1 + k_{-1}$ is rapid compared with the radical-pair decay rate, the amplitude of the delayed fluorescence at any time is proportional to the concentration of ^{1}(P$^+$I$^-$). The observation that the delayed fluorescence decay is roughly multi-exponential at low fields is a result of the fact that there is a broad distribution of ω values in the sample due to the distribution of hyperfine fields. If

there were only a single value of ω, the delayed fluorescence would oscillate at frequency ω. At very high field, ω is dominated by the g-factor difference: when $\Delta g \beta \, | \, B \, | / \hbar$ is large compared to the spread in ω from the hyperfine interaction, where B is the applied magnetic field, then the delayed fluorescence should oscillate (chemical quantum beats; see Ref. 19). While this work was in progress, quantum beats due to the Δg effect were reported for the recombination fluorescence from diphenylsulfide and para-terphenyl radical ions following electron irradiation in fluid solution at high field [20].

The expected delayed fluorescence time evolution at 1 kG, 50 kG and 150 kG based on the reaction scheme of Fig. 1 is shown in Fig. 2. These calculated decay curves are based on solutions to the stochastic Liouville equation discussed elsewhere [21] and use the isotropic value for Δg and other magnetic and kinetic parameters that are generally believed to be correct for quinone-depleted Rb. sphaeroides RCs. The calculated effects of variations of Δg, k_{-1}, and the exchange interaction, J, on the delayed fluorescence time evolution at 150 kG
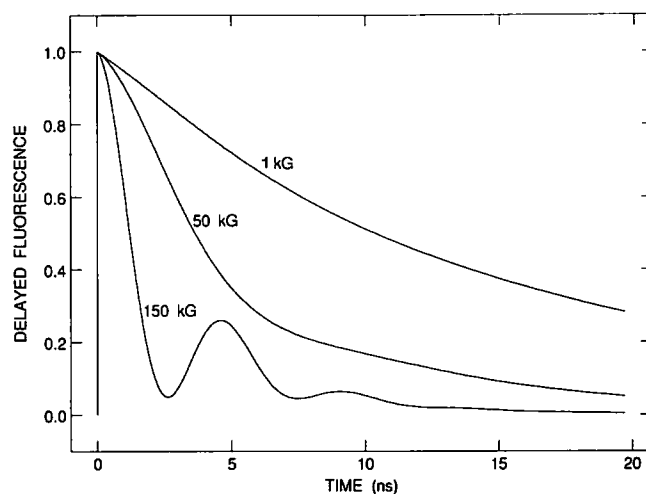

Fig. 2. Calculated delayed fluorescence as a function of time at 1, 50 and 150 kG, computed using the stochastic Liouville equation, as discussed by Goldstein and Boxer [21]. The parameters used are:

Parameter	Value
k_S	$5.0 \cdot 10^7 \text{ s}^{-1}$
k_T	$5.0 \cdot 10^8 \text{ s}^{-1}$
A(P$^+$)	9.5 G
A(I$^-$)	13.0 G
J	7.0 G
Δg	0.001

where A(P$^+$) and A(I$^-$) are the second moments of the hyperfine distributions of P$^+$ and I$^-$, respectively, J is the exchange interaction between the two unpaired electrons, Δg is the difference in g factors for P$^+$ and I$^-$, and k_S and k_T are the rate constants for the recombination paths shown in Fig. 1. These values are reasonable for Q$_A$-depleted RCs at room temperature [3,22–24]. The delayed fluorescence is assumed to be proportional to the concentration of ^{1}(P$^+$I$^-$).
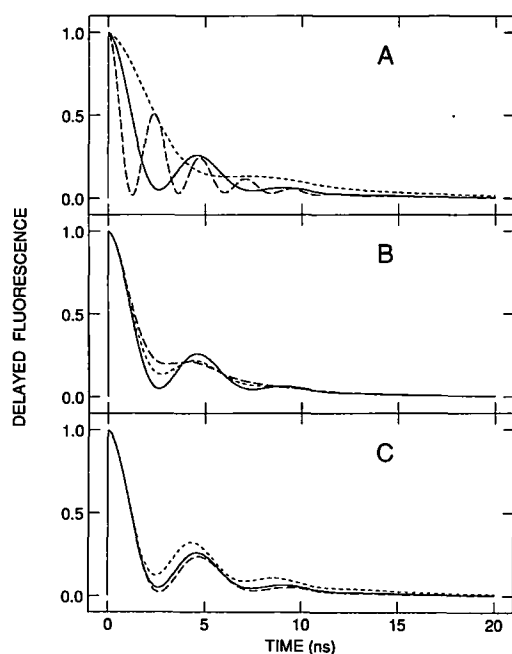
Fig. 3. Calculated effects of the kinetic and magnetic parameters on the expected time evolution of the delayed fluorescence at 150 kG. Unless stated, the parameter values listed in Fig. 2 are used, with $\Delta g = 0.001$, $k_{-1} = 0$, and $J = 7$ G. (A) Effect of Δg on the delayed fluorescence: the expected timed dependence is shown for Δg equal to 0.0005 (- - - - - -), 0.001 (———) and 0.002 (— — —). The frequency of the oscillations is proportional to Δg. (B) Effect of k_{-1} on the delayed fluorescence: the expected time dependence is shown for k_{-1} equal to 0 (———), $5 \cdot 10^8$ s^{-1} (- - - - -), and $1 \cdot 10^9$ s^{-1} (— — —). A large value of k_{-1} obscures the quantum beats, as the re-formation of ^{1}P interrupts the singlet-triplet mixing. k_{-1} cannot be much larger than approx. $1 \cdot 10^8$ s^{-1} without conflicting with the observed RYDMR linewidth [18]. (C) Effect of J on the delayed fluorescence: the expected time dependence is shown for J equal to 3.5 G (— — —), 7 G (———), and 14 G (- - - - -). Increasing J inhibits singlet-triplet mixing, causing an increase in the delayed fluorescence.

are shown in Fig. 3. k_{-1} must be finite in order for there to be delayed fluorescence. The case of $k_{-1} = 0$ in Fig. 3 illustrates the situation when the re-formation of ^{1}P is too slow to influence the singlet-triplet spin evolution. Changes in Δg affect the frequency of the quantum beats. Including a non-negligible k_{-1} causes a decrease in the amplitude of the oscillations, as the phase relationship between the two unpaired electrons in P$^+$I$^-$ during the singlet-triplet evolution is interrupted by re-formation of ^{1}P. An increase in the exchange interaction decreases the efficiency of singlet-triplet mixing, causing an increase in the total delayed fluorescence without a significant change in the magnitude of the beats. For an oriented sample, inclusion of the electron–electron dipole–dipole interaction would have the same effect as changing the exchange interaction. The range of parameter values used to generate the plots in Fig. 3 is larger than is reasonable given the information known about the radical-pair state. Beats should be observed for all reasonable values of the relevant parameters, as discussed further below. The

sensitivity of the oscillations to the parameters motivated our experiments.

These calculations use the isotropic value for Δg. The situation is more complicated because the g factors are tensor quantities; consequently, the value of ω will depend on the orientation of the RC relative to the external magnetic field. Although the anisotropy in the g factors may be small, the anisotropy may still be large relative to Δg [6]. The observation that the anisotropy in the quantum yield of ^{3}P is large at high field [25] provides further evidence of the tensor nature of Δg. It is only at very high magnetic fields with an oriented sample that there will be a sharp distribution of singlet-triplet mixing rates. For this reason, we measured the time-evolution of the delayed fluorescence of Q$_A$-depleted RCs oriented in dried phosphatidylcholine vesicles in magnetic fields from 1 kG to 150 kG. We did not observe quantum beats; the absence of beats suggests that the scheme of Fig. 1 is not complete. This result is used to support an alternative reaction scheme discussed in the accompanying paper [18].

The time evolution of the delayed fluorescence at very high field can, in addition, provide a direct measure of k_T. At 1 kG, ω is slow relative to k_S and k_T, so the radical pair decays predominantly through the slower k_S path. In the limit of very low ω, the fluorescence lifetime would be at the maximum value of k_S^{-1}. As the externally applied magnetic field is increased, ω increases, there is more equilibration between the singlet and triplet radical-pair electronic spin states, and more of the radical pairs decay through the faster k_T path. These effects will cause a reduction in the yield and lifetime of the delayed fluorescence. In the limit of infinite ω, the lifetime of the delayed fluorescence will reach the minimum value of $2(k_S + k_T)^{-1}$. While k_S is known quite accurately from measurements of the effect of magnetic fields on the radical-pair decay rate [15], values of k_T in the range $(2-6) \cdot 10^8$ s^{-1} have been derived indirectly from reaction-yield detected magnetic resonance (RYDMR) linewidth measurements [24,26,27] using the assumption that other sources of dephasing of the electron spin correlation in the radical-pair state, including k_{-1} and k_S and any power-broadening effects, were slow relative to k_T. This analysis is complicated, and there is some disagreement about the correct interpretation of the data. Because any dephasing factors that were neglected would increase the RYDMR linewidth, this analysis possibly overestimates k_T. In contrast, in the infinite-field limit, k_T can be measured directly by monitoring the time evolution of the delayed fluorescence. Earlier observations of the magnetic field effect on the quantum yield and decay rate of ^{3}P indicate that this limit is approachable for field strengths in excess of 100 kG [25]. As described below, we observe a saturation of the magnetic field effect on the delayed fluorescence by 150 kG. The

measurements described here furnish a value for k_T of $(4.0 \pm 0.3) \cdot 10^8$ s^{-1}. As discussed in the accompanying paper, the actual value of k_T has significant implications for the evaluation of alternative reaction schemes [18].

Materials and Methods

Quinone-depleted RCs from *Rb. sphaeroides* R-26 mutant were prepared by standard procedures [13,28] and were dialized against buffer (10 mM-Tris/0.4% cholate (pH 8.0)). Vesicles were prepared following the procedure of Nabedryk and co-workers [29] following modifications suggested by Breton (Breton, J., personal communication). Egg phosphatidylcholine (PC) in hexane was dried and mixed in Tris buffer (10 mM PC in 10 mM Tris (pH 8.0)) and deoxygenated with Ar. Vesicles were formed by sonicating under Ar until the suspension was clear. The RCs were added (RC/PC (1:1, w/w)), and the solution was then dialyzed against 10 mM Tris buffer overnight to remove the cholate. The solution was then spun at 100 000 × g to pellet out the vesicles. The pellet was resuspended in distilled water, respun, resuspended, concentrated, and then dried on clean glass slides. The linear dichroism to absorbance ratio was used to determine the degree of orientation. The value of this ratio at 760 nm ($S = 0.24$) indicated an angle between the transition dipole moment for this absorption band the normal to the slide of approx. 45°C, in agreement with literature values for oriented samples [30]. Eight slides were stacked together.

A time-resolved single-photon counting apparatus was set up around an open-bore superconducting magnet at the Francis Bitter National Magnet Laboratory. Good reviews of time-resolved single-photon fluorescence techniques and data analysis methodology can be found elsewhere [31]. Due to the magnet geometry, we used an in-line excitation-detection geometry. Direct excitation of P was achieved by a pulsed diode laser (Newport Corporation LD-10; 850 nm, 200 ps FWHM, 20 μW, 100 kHz repetition rate). The excitation light was filtered by an 850 nm interference filter to remove a small longer-wavelength component. The sample was placed between crossed infrared film polarizers to block the excitation light from the detector, with the glass slide normal to the magnetic field axis and the light propagation direction. The sample had a total optical absorbance at 800 nm of approx. 8. The large optical absorbance was used in order to reduce the amount of scattered laser light reaching the detector. There is a large Stokes shift in the ^{1}P state, so the optical absorbance of the sample at the wavelength of the peak of the fluorescence at 910 nm was approx. 1. This large Stokes shift, combined with the very small delayed fluorescence quantum yield (about 10^{-4}) makes the probability of a photon due to fluorescence being ab-

sorbed and re-emitted at a later time less than 0.1%. The sample was allowed to equilibrate with the temperature of the inner bore of the magnet ($-4°$C, as measured by a thermocouple). The fluorescence was filtered with two sharp cut-off 900 nm long-pass filters and was directed to the photomultiplier tube (PMT, Hammamatsu 1828-S1) with a quartz light pipe. Insertion of a 900 nm interference filter did not change the time evolution. 4096 channels of data were collected at 40 ps per channel. Approx. $2 \cdot 10^5$ total counts were recorded for each measurement. The data collection was always in the low-count limit (under 0.1%). The instrument response function was measured with the sample and crossed polarizers replaced by a diffuse scatterer. The instrument showed a FWHM of approx. 1.7 ns.

Results

Fluorescence decays at 1, 50 and 150 kG, and the instrument response function are shown in Fig. 4, with the amplitude of the signals normalized to the amount of prompt signal calculated with the fitting program. As shown, there is a large delayed fluorescence component with a significant magnetic field dependence. The anticipated quantum beat phenomenon was not observed at any field; possible reasons for this are discussed below. The bump in the signal at 20 ns is due to an afterpulse of the photomultiplier tube and was present in the instrument response function as well as the delayed fluorescence signal.

We tried to approach the modelling of time dependence of the delayed fluorescence with as few assumptions as possible. Because the signal appeared to be roughly exponential, our first attempt was to fit the
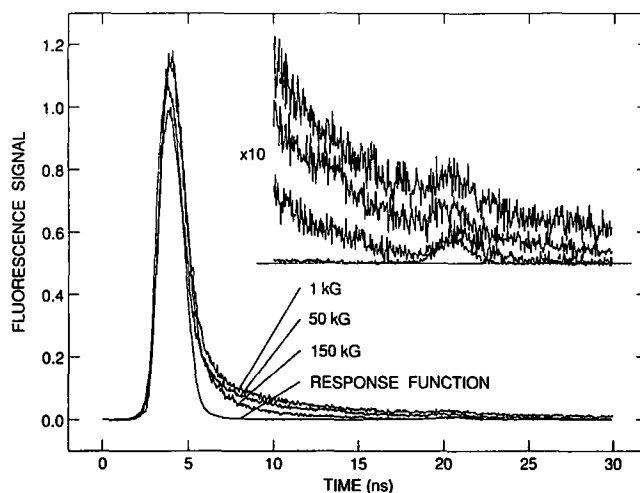

Fig. 4. Observed delayed fluorescence signals at 1, 50 and 150 kG for oriented Q_A-depleted *Rb. sphaeroides* R-26 RCs at $-4°$C, along with the instrument response function, all normalized to the amount of prompt signal as calculated by deconvolution with the response function. The bump at about 20 ns is an afterpulse of the photomultiplies tube and is present in all signals.

signal to the convolution of the response function with a continuous distribution of exponentials plus a prompt component [32]. At all fields, the fits to continuous distributions resulted in two or three well-resolved lifetime components. These components could be followed as a function of applied magnetic field. At 1 kG, three resolvable components resulted from the fit. As the field is increased, the two shorter-lifetime components coalesce, combining to form only one resolvable component by 50 kG. Higher fields result in the resolution of two components. The most dramatic magnetic field effect is on the lifetime of the longest-lived component, which shows a steady decrease with field, with the magnetic field effect eventually saturating at the very highest fields. The reduced χ^2 values averaged approx. 1.4. We next fit the signal to the convolution of a finite number of exponentials plus a prompt component with the instrument response function. Again, the reduced χ^2 values averaged approx. 1.4. In all cases, the fits to the finite number of exponentials resulted in fits as good as those achieved using continuous distribution of exponentials. The number, lifetimes and amplitudes of the descrete components required for a best fit correlated with the number, lifetime and amplitude of the resolvable components in the continuous distribution analysis. The results of the descrete lifetime analysis were qualitatively and quantititatively similar to the results from the continuous distribution analysis. For these reasons, the following discussion will be based on the descrete lifetime component analysis, as has been done in previous work [11,16,17].

The lifetimes of the decay components at various fields are shown in Fig. 5A. The data at magnetic fields higher than 25 kG were fit with two exponentials, while the data at 1 kG and 25 kG were fit by three exponentials. The lifetime of the longest-lived component is seen to shorten considerably as the field is increased. The yields of the various components along with the total delayed fluorescence yield are shown in Fig. 5B. The yields are equal to the amplitude of the lifetime component times the lifetime of that component, normalized to the amount of prompt fluorescence. The yield of the longest component, as well as the total delayed fluorescence yield, also decreases at higher fields. The uncertainties in both lifetime (± 0.3 ns) and relative yield (± 0.02) are based on the spread in these values obtained using data from three separate measurements at both 50 kG and 100 kG.

The results at 1 kG are similar to those observed by other investigators with a room-temperature isotropic sample in aqueous buffer at 600 G. Woodbury and co-workers obtained adequate fits to their data with three exponentials; two of the lifetimes observed here (1.4 $\pm$ 0.3 ns and 4.6 $\pm$ 0.3 ns) are similar to two of the components that they observed in Q_A-reduced (1.02 $\pm$ 0.05 ns and 4.1 $\pm$ 0.4 ns [11]) and Q_A-depleted RCs
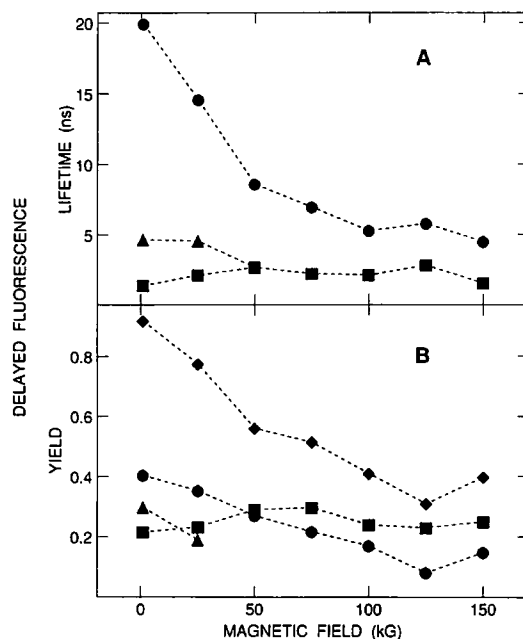

Fig. 5. (A) Lifetimes of the delayed fluorescence decay components as a function of external magnetic field. The data at 50 kG and above can be fit by two exponentials; a fast component (■) and a slow component (●). The data below 50 kG require the addition of a third middle component (▲). Experimental uncertainties are estimated by the spread in fit values for three independent measurements at both 50 and 100 kG and are comparable to the size of the symbols (± 0.3 ns). The lifetimes of different components as a function of magnetic field were tracked by observing the magnetic field dependence of the well-defined components obtained by fitting the decay curves to a continuous distribution of lifetimes, as detailed in text. (B) Yields of the delayed fluorescence decay components as a function of external magnetic field. Shown are the total integrated yields of the various components, equal to the initial amplitude times the lifetime of that component, normalized to the prompt fluorescence yield, for the fast component (■), the slow component (●), the third middle component required below 50 kG (▲), as well as the total delayed fluorescence yield (♦). Experimental uncertainties calculated as described in (A) are comparable to the size of the symbols (± 0.02).

(0.94 ns and 3.3 ns [17]). The third component is significantly longer (19.9 $\pm$ 0.3 ns vs. 11.6 $\pm$ 0.7 ns for Q_A-reduced or 15.0 ns for Q_A-depleted). Woodbury and co-workers observed a strong temperature dependence to the lifetime of the longest component, with the lifetime doubling as the temperature was reduced from room temperature to 200 K [11,17]. This temperature-dependence presumably reflects the temperature-dependence of k_S, and likely explains why the observed lifetime of the longest-lived component in our $-4°$C sample (19.7 ns) is longer than for their room-temperature samples (15 ns). The magnitudes of the three components relative to the prompt flouorescence are also comparable to their measurements; the relative yields for the three components in this work are 0.22 $\pm$ 0.02, 0.30 $\pm$ 0.02, and 0.40 $\pm$ 0.02 compared to the values obtained by Woodbury and co-workers (0.12, 0.34 and 0.44 for Q_A-reduced RCs [11], and 0.40, 0.28 and

0.31 for Q_A-depleted RCs [17] (the large magnitude of the fastest decay component in their measurement on Q_A-depleted RCs was ascribed to possible sample contamination). Hörber and co-workers could distinguish only two components at room temperature apart from prompt fluorescence, with lifetimes of 2 ns and 11 or 12 ns, depending upon whether the quinone was reduced or removed, respectively [16]. The relative yields of these components were also comparable to those obtained here. It is important, however, 'to note that the oriented dried vesicle samples we are using and the isotropic aqueous sample used by Woodbury, Hörber and their co-workers may have different properties. Woodbury and Parson found significant differences in the delayed fluorescence amplitudes depending upon the conditions of the sample, including RC concentration, detergent concentration, and presence of glycerol [11]. In light of this large (and unexplained) variability, we consider the values we obtained at 1 kG to be in good agreement with the earlier work. Both the other groups reported that only the slowest component was significantly affected by the magnetic field. Fig. 5 shows that the dominant magnetic field effect continues to be for the slowest component at higher field.

Discussion

The value of k_T

As discussed in the Introduction, the rate of decay of the delayed fluorescence can furnish the rate of decay of $^3(P^+I^-)$. In the limit of ω very slow relative to k_S and k_T, the fluorescence lifetime would be at the maximum value of k_S^{-1}. The singlet-triplet mixing rate is lowest at about ¯1 kG. The theoretically predicted delayed fluorescence time evolution at 1 kG shown in Fig. 2 can be best fit by a single exponential of lifetime 16 ns (not shown), slightly shorter than the value of k_S^{-1} used to generate the decay (20 ns) and similar to the lifetime of the longest-lived delayed fluorescence component in Q_A-depleted RCs as measured by Woodbury and Parson [11] at room temperature. The shorter lifetime of this component in Q_A-reduced RCs possibly reflects the faster singlet-triplet mixing rate in these RCs due to coupling of the unpaired electron on I^- with the unpaired electron on Q_A^-. Measurements of the radical-pair decay rate by transient absorption at different temperatures and fields in Q_A-reduced RCs performed by Schenck and co-workers [13] indicate a value for k_S^{-1} at $-4°C$ of approx. 25 ns. The lifetime of the longest-lived component that we observe in Q_A-depleted RCs at this temperature (19.9 ± 0.2 ns) is again slightly shorter.

In the limit of infinite ω, the lifetime of the fluorescence would reach the minimum value of $2(k_S + k_T)^{-1}$. Saturation of the effect of the external magnetic field on the delayed fluorescence decay is achieved by 100 kG (Fig. 5). The lifetime of the longest component at 150

kG is 4.5 ± 0.3 ns, indicating a value for k_T of $(4.0 \pm 0.3) \cdot 10^8 \, s^{-1}$. This is within the range of $k_T = (2-6) \cdot 10^8 \, s^{-1}$ derived from an analysis of the RYDMR data [24,26,27]. If the shorter-lived delayed fluorescence components were included in the analysis, the value of k_T increases to $9.3 \cdot 10^8 \, s^{-1}$. Since this is larger than compatible with the RYDMR data, this is an indication that the shorter components are not due to the state that this undergoing singlet-triplet mixing. The temperature-independence of the RYDMR linewidth and the shape of the magnetic field effect at low field are an indication that k_T is not strongly dependent on temperature [26].

Absence of quantum beats

The absence of structure in the delayed fluorescence time evolution at 150 kG is in conflict with the predictions shown in Fig. 2 and 3, based on the reaction scheme in Fig. 1. This could be either the consequence of an imperfect experiment or an indication that the reaction scheme is not correct.

It is impossible to verify by linear dichroism measurements that complete orientation of the RCs has been obtained. While our linear dichroism measurements agree with the values obtained by others using similar orientation techniques, there still may be a residual distribution of orientations (mosaic spread). This problem could be solved in principle by performing the fluorescence experiment at very high field on a single crystal. The predicted delayed fluorescence time evolution shown in Fig. 2 is based on the isotropic values of the magnetic parameters. These values may not be completely accurate for a sample with a fixed orientation with respect to the external magnetic field. Changes in the parameter values might cause the predicted beats to be obscured. The delayed fluorescence predicted by the model calculations presented in Fig. 3 were convolved with the instrument response function in order to test the range of parameters that would yield observable quantum beats. Assuming that the reaction scheme in Fig. 1 is correct, such beats would be observed for $k_{-1} < 1 \cdot 10^9 \, s^{-1}$, $J < 100$ G, and $0.0005 < \Delta g < 0.002$. A value of k_{-1} larger than about $1 \cdot 10^8 \, s^{-1}$ would be incompatible with the RYDMR linewidth given the value of k_T derived from the 150 kG delayed fluorescence time evolution. J has been estimated to be about 7 G on the basis of the effect of magnetic fields on the quantum yield of ^3P [22]. The value of Δg that is relevant for the oriented sample is somewhat uncertain. The anisotropy in the g factor for P^+ has been measured by the angular dependence of the EPR signal in single crystals of Rb. sphaeroides [33] and is found to be very small, as expected for a radical where the g factor is near to the free electron value. Comparable measurements have not been reported for I^-. In addition, it is not clear how accurately the g values of the long-lived,
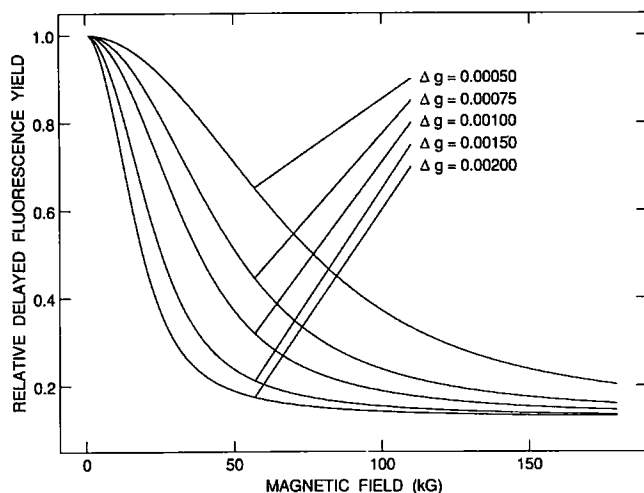
Fig. 6. Effect of Δg on the relative delayed fluorescence yield, calculated using the other parameter values listed in the caption to Fig. 2 (see footnote, this page). As shown by comparison with the data contained in Fig. 5, Δg is approximately equal to 0.001. This indicates that the quantum beats are not obscured by Δg being too large or too small.

trapped P^+ or I^- radical states studies by EPR reflect the g values of the radicals on the nanosecond time-scale. The shape of the magnetic field dependence of the delayed fluorescence yield, however, is a sensitive measure of Δg for the sample. Fig. 6 shows the effect of variations of Δg on the calculated magnetic field dependence of the relative delayed fluorescence yield, using the other parameters listed in the caption to Fig. 2. * Comparison of these results with the experimental data in Fig. 5 indicates that Δg is close to 0.001 for the oriented sample, and is not likely to be smaller than 0.0005 nor larger than 0.002. This indicates that the values of the parameters are in the range necessary for beats to be observed, if the reaction scheme is correct.

The second possibility is that the reaction scheme of Fig. 1 needs revision. As shown in Fig. 2, the model based on the reaction scheme predicts a roughly single exponential delayed fluorescence decay at 1 kG, in contrast to the observations of Woodbury and Parson [11], Hörber et al. [16], and the data in Fig. 5. The fact that the fast components are relatively magnetic-field-independent suggests that these components may not involve the state that undergoes magnetic-field dependent singlet-triplet mixing. There have been indications that the scheme is inadequate in explaining a wide variety of other experimental observations [18]. In par-

ticular, it has been postulated that intermediate states may exist on the route to formation of $^1(P^+I^-)$ from ^1P [35], possibly involving the initial formation of a form of the radical pair state which does not undergo singlet-triplet mixing, followed by nuclear coordinate relaxation on a nanosecond time scale to a form which does [11]. If this is the case, there will be an exponential rate of formation of $^1(P^+I^-)$ and a resulting distribution of starting times for the singlet-triplet evolution. If this distribution is on the order of the time-scale for the spin evolution (ns), any coherent effects will be damped out; this could explain the absence of quantum beats at high magnetic field strength. This proposal is discussed in more detail and with other available data in the accompanying paper [18].

Conclusions

Much of the information about the magnetic interactions in the radical-pair state has come indirectly through the use of theoretical models that can mimic the experimentally observed magnetic field effect data. This often involves a series of approximations, simplifications, and a number of adjustable parameters whose effects may be complicated and non-intuitive, especially in the low-field regime (under 1 kG). The delayed fluorescence is one of the few ways of observing the time evolution of the electronic spin state of the radical pair directly. Observation of quantum beat structure in the delayed fluorescence at very high field would have been a dramatic confirmation of the applicability of the radical-pair mechanism theory and the reaction scheme. Furthermore, as demonstrated in Fig. 3, the frequency of the beats and the amplitude variation would provide a direct measurement of a number of important magnetic and kinetic parameters. The absence of quantum beats can be explained by a few factors, including the possibility that the reaction scheme shown in Fig. 1 is incomplete, a conclusion we derive from independent evidence in the accompanying paper [18]. Even without the observation of quantum beats, it is possible to obtain the values of the rate constants k_S and k_T. k_S is known from measurements of radical-pair lifetimes as a function of magnetic field by transient absorption spectroscopy, but k_T up to now has been known only indirectly through analysis of the RYDMR lineshape [24,26,27]. As shown in the accompanying paper, lower values of k_T (less than $2 \cdot 10^8$ s^{-1}) would allow the resolution of a number of discrepancies between theoretical models and experimental observations [18]. Such lower values would be compatible with the RYDMR linewidth if there were other electron spin dephasing processes present in the radical-pair state. The value found here, $(4.0 \pm 0.3) \cdot 10^8$ s^{-1}, is within the range of values estimated from the RYDMR linewidth analysis without consideration of other dephasing processes,

---

* Because the delayed fluorescence yield is proportional to the time integral of the $^1(P^+I^-)$ concentration, as is the quantum yield of the ground state formed by decay of the radical-pair state through k_S, the delayed fluorescence yield should be proportional to $(1 - \Phi_{^3P})$, where $\Phi_{^3P}$ is the quantum yield of ^3P. Calculations of the relative delayed fluorescence yield are therefore a simple extension of methods developed for calculating ^3P quantum yields [34].

$(2-6) \cdot 10^8$ s^{-1}, and is too high to resolve these discrepancies.

References

1 Woodbury, N.W., Becker, M., Middendorf, D. and Parson, W.W. (1985) Biochemistry 24, 7516–7521.
2 Martin, J.-L., Breton, J., Hoff, A.J., Migus, A. and Antonetti, A. (1986) Proc. Natl. Acad. Sci. USA 83, 957–961.
3 Boxer, S.G., Chidsey, C.E.D. and Roelofs, M.G. (1983) Annu. Rev. Phys. Chem. 34, 389–417.
4 Werner, H., Schulten, K. and Weller, A. (1978) Biochim. Biophys. Acta 502, 255–268.
5 Haberkorn, R. and Michel-Beyerle, M.E. (1979) Biophys. J. 26, 489–498.
6 Boxer, S.G., Chidsey, C.E.D. and Roelofs, M.G. (1982) Proc. Natl. Acad. Sci. USA 79, 4632–4636.
7 Shuvalov, V.A. and Klimov, V.V. (1976) Biochim. Biophys. Acta 440, 587–599.
8 Godik, V.I. and Borisov, A.Y. (1980) Biochim. Biophys. Acta 548, 296–308.
9 Godik, V.I. and Borisov, A.Y. (1980) Biochim. Biophys. Acta 590, 182–193.
10 Van Bochoven, A.C., Van Grondelle, R. and Duysens, L.N.M. (1981) in Procedings of 5th International Congress on Photosynthesis (Akoyunoglou, G., ed.), International Science, Jerusalem.
11 Woodbury, N.W. and Parson, W.W. (1984) Biochim. Biophys. Acta 767, 345–361.
12 Rockley, M.R., Windsor, M.W., Cogdell, R.J. and Parson, W.W. (1975) Proc. Natl. Acad. Sci. USA 72, 2251–2255.
13 Schenck, C.C., Blankenship, R.E. and Parson, W.W. (1982) Biochim. Biophys. Acta 680, 44–59.
14 Tang, J. and Norris, J.R. (1982) Chem. Phys Lett. 92, 136–140.
15 Chidsey, C.E.D., Kirmaier, C., Holten, D. and Boxer, S.G. (1984) Biochim. Biophys. Acta 766, 424–437.
16 Hörber, J.K.H., Göbel, W., Ogrodnik, A., Michel-Beyerle, M.E. and Cogdell, R.J. (1986) FEBS Lett. 198, 273–278.
17 Woodbury, N.W., Parson, W.W., Gunner, M.R., Prince, R.C. and Dutton, P.L. (1986) Biochim. Biophys. Acta 851, 6–22.
18 Goldstein, R.A. and Boxer, S.G. (1989) Biochim. Biophys. Acta 977, 78–86.
19 Boxer, S.G., Goldstein, R.A. and Franzen, S. (1988) in Photoinduced Electron Transfer (Fox, M.A. and Chanon, M., eds.), Vol. B, p. 163–215, Elsevier, Amsterdam.
20 Veselov, A.V., Melekhov, V.I., Anisimov, O.A. and Molin, Yu.N. (1987) Chem. Phys. Lett. 136, 263–266.
21 Goldstein, R.A. and Boxer, S.G. (1987) Biophys. J. 51, 937–946.
22 Hoff, A.J. (1986) Photochem. Photobiol. 43, 727–745.
23 Lersch, W. and Michel-Beyerle, M.E. (1983) Chem. Phys. 78, 115–126.
24 Norris, J.R., Bowman, M.K., Budil, D.E., Tang, J., Wraight, C.A. and Closs, C.L. (1982) Proc. Natl. Acad. Sci. USA 79, 5532–5536.
25 Goldstein, R.A., Takiff, L. and Boxer, S.G. (1988) Biochim. Biophys. Acta 934, 253–263.
26 Möhl, K.W., Lous, E.J. and Hoff, A.J. (1985) Chem. Phys. Lett. 121, 22–27.
27 Hunter, D.A., Hoff, A.J. and Hore, P.J. (1987) Chem. Phys. Lett. 134, 6–11.
28 Okamura, M.Y., Issacson, R.A. and Feher, G. (1975) Proc. Natl. Acad. Sci. USA 72, 3491–3495.
29 Nabedryk, E., Tiede, D.M., Dutton, P.L. and Breton, J. (1982) Biochim. Biophys. Acta 682, 273–280.
30 Verméglio, A. and Clayton, R.K. (1976) Biochim. Biophys. Acta 449, 500–515.
31 Yguerabide, J. (1972) Methods Enzymol. 26C, 498–578.
32 Ware, W.R., Doemeny, L.J. and Nemzek, T.L. (1973) J. Phys. Chem. 77, 2038–2048.
33 Allen, J.P. and Feher, G. (1984) Proc. Natl. Acad. Sci. USA 81, 4795–4799.
34 Chidsey, C.E.D., Roelofs, M.G. and Boxer, S.G. (1980) Chem. Phys. Lett. 74, 113–118.
35 Haberkorn, R., Michel-Beyerle, M.E. and Marcus, R.A. (1979) Proc. Natl. Sci. USA 76, 4185–4188.